The Journal of Chemical Physics ARTICLE pubs.aip.org/aip/jcp

Response of a ODT monolayer to rapid heating studied by vibrational sum frequency spectroscopy

Cite as: J. Chem. Phys. 164, 124703 (2026); doi: 10.1063/5.0321396
Submitted: 7 January 2026 • Accepted: 6 March 2026 •
Published Online: 23 March 2026

Matthias Linke and Eckart Hasselbrink[a)]

AFFILIATIONS

Fakultät für Chemie and Center for Nanointegration (CENIDE), Universität Duisburg-Essen, D-45117 Essen, Germany

[a)]Author to whom correspondence should be addressed: Eckart.Hasselbrink@Uni-Duisburg-Essen.de

ABSTRACT

A self-assembled monolayer of octadecanethiol adsorbed on a thin film of Au was flash-heated by illuminating the structure, further consisting of a glass substrate and a Ti contact layer, with a 19 ps laser pulse of 532 nm light from the backside, inducing a temperature increase by 113 K within 100 ps. The details of the temporal evolution of the temperature can be well modeled when taking into account the predominant light absorption in the Ti layer and the large thermal boundary resistance between the layers. The evolution of the molecular structure is time-resolved by vibrational sum frequency spectroscopy. While the molecules are initially tilted by 30° with respect to the surface normal, this order is rapidly lost, whereby the disordering lags 150 ps behind the temperature evolution. After 400 ps, the molecular order is dissolved.

I. INTRODUCTION

Self-assembled monolayers (SAMs) formed from alkanethiols on a gold surface are the most extensively studied system of organic molecular monolayers.[1–3] This system was—to the best of our knowledge—discovered in 1983 by Nuzzo and Allara.[4] *n*-alkylthiols with a number of carbon atoms between 12 and 20 generally form spontaneously well-ordered layers on carefully prepared gold films, as the latter exhibit large areas of (111) structure.[5]

This system has been characterized using a variety of techniques. They include, among others, transmission electron spectroscopy,[6] infrared spectroscopy,[7] optical ellipsometry,[8] helium beam diffraction,[9] high-resolution electron energy loss spectroscopy,[10] scanning tunneling microscopy,[11] and x-ray diffraction.[12] Although it is tempting to assume that the structure is of $(\sqrt{3} \times \sqrt{3})$ R30° symmetry, as this is the one of the highest symmetry consistent with an epitaxial densely packed arrangement of the molecules, experimental evidence suggests the coexistence of two subsets of molecules coexisting in a super-structure commonly referred to as $c(2 \times 4)$[13,14]—presumable a four alkyl chain per unit cell structure. From grazing incidence x-ray diffraction (GIXD), it was inferred that the alkyl chains are tilted by ~30° with respect to the surface normal toward their next nearest neighbors.[15–17] The chains are tilted because the optimal spacing of Au–S bonds is larger than the van der Waals radius of the alkyl chain. Hence, they lean over until tight contact with the neighbor is established. Despite all the effort, still open questions remain, in particular regarding the role of structural defects in the dynamics at temperature changes.[18–20]

The response of alkanethiol monolayers to changes in temperature was studied experimentally[13] and theoretically.[21] Monte Carlo modeling suggests that when elevating the temperatures between 300 and 400 K, the thermal motions become so large that the alkyl chains no longer lean against each other anymore, but rather, the individual molecules carry out pendulum motions. At 400 K, the mean tilt angle is then 0°. GIXD for a decanethiol monolayer showed that at this temperature, the layer is molten but the molecules do not yet desorb.[22]

Vibrational sum frequency spectroscopy (vSFS) is a versatile tool to study molecular monolayers because of its surface selectivity and inherent strict selection rules.[23] A welcome effect of the selection rules is that the complexity of the spectrum is reduced when compared to IR absorption spectroscopy and that choosing certain combinations of the polarization of the three light waves involved

allows us to shed light on the adsorption geometry of the molecules, in particular when studying well-ordered systems. These advantages were exploited by several groups to study alkanethiol monolayers on Au.[13,24,25]

In this paper, we report on the response of an octadecanethiol (ODT) monolayer on Au to a 20 ps heating pulse. A 532 nm laser pulse of this length heats a Ti metal from the back side, which transfers heat to a 13/30 nm Ti/Au film structure. Over the course of 100 ps, a transient temperature rise is induced at the surface, onto which the SAM is coupled. We observe that with a time lag of 125 ps, the molecular system responds. After a time of 400 ps, the molecular order is dissolved. Data for different polarization combinations and the symmetric and anti-symmetric CH_3 stretch were used to shed light on the evolution of the adsorption geometry and surface order. With this study, we continue earlier work that studied the response of 4-nitrothiophenol.[26]

In a seminal work, Dlott and co-workers[27,28] reported on the flash-heating of alkylthiolates on Au(111) using fs laser pulses that, for a 16 C-atom alkylthiol, the methyl end groups show after ~2.7 ps the first response, which thereafter progresses with a time constant of ~8 ps. Extending this study to alkylthiols of different lengths showed a scaling of the response time with the latter. In this paper, we focus on the time-evolution of the molecular adsorption geometry and discuss it not only in terms of a mean tilt angle but also of the evolution of the spread of individual ones, which reflects the degree of order.

II. EXPERIMENTAL

A commercial pulsed ps laser system (Ekspla PL2231) together with a tunable OPA/DFG stage (Ekspla PG501DFG) was used to build a scanning vSF spectrometer with ~12 cm^{-1} resolution. Tunable IR (3.3–3.5 μm) and 532 nm light pulses of 19 ps duration at a repetition rate of 50 Hz were employed in the experiment. Pulse energies of 280 μJ (532 nm) and 10–30 μJ (IR) were employed. The 532 nm laser beam was split into two portions (50:50): one was used for upconversion in the vSFS, while the other was used for flash-heating the sample.

The samples, 10 × 10 mm^2, were prepared at the local optics shop using commercially available glass cover slips (Menzel-Gläser 1, thickness: 0.19–0.23 mm) as substrates onto which, first, a 13 nm thick contact adhesion layer of Ti, and then a 30 nm thick Au film was deposited. Details of the monolayer preparation were reported before.[29] The IR and upconversion light beams were directed at the front of the sample under incident angles of 44° and 54°, respectively, and had on the surface spot sizes (FWHM) of 1.2 and 1.9 mm, respectively.

A home-built sample stage was employed that allowed us to direct a 532 nm laser beam onto the backside of the sample at normal incidence. This beam served to heat the metal layers at the sample top. Its diameter was larger than that of the beams used in the vSFS. Less than 10% of the 532 nm light penetrates through the film structure. The probe spot was placed off-center, and the sample slowly rotated around its center normal, such that, over time, different areas were utilized for the experiment.

The experiment requires a reading of the sample surface temperature with the time resolution of the laser system, namely, ~10 ps. Following earlier work in the literature, we used the change in reflectivity as a proxy for the temperature.[30] For this purpose, the reflected intensity of the 532 nm light used for upconversion was utilized and normalized to the incoming intensity. This measurement was calibrated with equivalent measurements when statically heating the sample.

A translation stage with 8 fs resolution was used to control the delay between the heating and probing laser pulses. For each data point, typically 361 laser pulses were sampled and averaged. At each delay line position, two spectra were recorded, one with the flash-heating laser pulse blocked by a shutter and another with the light passing through this shutter. This allows us to rule out misleading effects from degradation of the sample over the long course of an experimental run (up to 24 h). To monitor the reproducibility of the flash-heating, the incoming and reflected intensities of the upconversion beam were recorded together with the vSFS spectra for both situations.

For the IR light, only the *p* polarization was used, adjusted using a $\lambda/2$-plate. The 532 nm light used for upconversion passes through a combination of two Brewster type thin film polarizers and a $\lambda/2$ plate to control intensity and polarization. The polarization of the detected SF light is defined by a polarizer placed in front of the photomultiplier registering the signal. It was verified that switching between the polarization combinations did not alter the sensitivity by more than 7%.

The spectra were fit using the following established expression:[23,31]

$$I^{SFS}(\omega_{IR}) \propto \left| \left|\chi^{(2)}_{NR}\right| + \sum_i e^{-i\xi_i} \frac{A_i}{\omega_{IR} - \omega_i + i\Gamma_i} \right|^2, \quad (1)$$

where $\chi^{(2)}_{NR}$ is the second order susceptibility leading to a non-resonant background due to the interband transition in Au. A_i, ω_i, and Γ_i are the vSF line strength, the position, and the width (HWHM) of the vibrational resonance *i*, respectively. ω_{IR} is the frequency of the incident IR light. The parameters are real and always have a positive value in our model. ξ_i is the phase difference between the non-resonant background and the molecular susceptibility.

Fitting the experimental spectra with this model allows us to extract the *A* and Γ values for all identified modes and to use these to calculate a hypothetical spectrum that would be observed if the non-resonant background were not present. The intensity of a mode in this spectrum, $|A/\Gamma|^2$, is what we refer to as the *molecular intensity*.

It is well-established knowledge that the set of fit parameters is not unique in the case that a non-resonant background is present.[32] In fact, up to $2(N-1)$ sets exist that each result in the identical fit curve, where *N* is the number of resonances. To overcome this ambiguity, we have rigorously calculated the phases of the various resonances. However, these depend on the tilt angle of the symmetry axis of the molecular groups, CH_2 and CH_3, with respect to the surface normal. For the detailed results, the reader is referred to the supplementary material. It is important to note that the tilt angles of the symmetry axes of the molecular groups are not identical to the one of the molecular axis in the all-trans configuration. The results suggest that the anti-symmetric stretches of CH_2 and CH_3 share the same phase, irrespective of the polarization combination. The same is true for the symmetric stretch in the *ssp* combination, while small differences are calculated for the *ppp* combination. However, these differences are too small to significantly influence the fits, given the

experimental uncertainties. The offspring are such that the phase difference between the different modes can be regarded as independent of the tilt angle. Only one phase difference, namely, the one of the set of molecular stretching vibrations with respect to the non-resonant background, is undetermined and treated as a free parameter.

III. RESULTS

A. Sample heating

As detailed in a previous publication,[26] the change in reflectivity of the sample surface for 532 nm light with temperature[30] was used to access the transient sample surface temperature. Figure 1 displays the recorded development of the sample temperature when flash heating the sample. A temperature jump exceeding 100 K is observed. After about 500 ps, the observed temperature slowly decreases again.

The basic model describing the heating of a metal surface by pulsed laser excitation is well established[33] and experimentally verified.[34] In order to analyze the result here, however, we need to consider the optical and electronic properties of the layered structure and the fact that it is illuminated from the backside. The penetration depth for 532 nm light is ~13 nm in Ti and ~20 nm in Au. Hence, the heating light is predominantly absorbed in the 13 nm thick Ti film. Ti also has the larger electron–phonon coupling constant, G.[35,36] Consequently, the laser energy is predominantly absorbed in the Ti film and converted into local heat such that the Ti film is initially hotter than the Au top layer. Heat conduction and, to a smaller extent, hot electron diffusion in the two-layer system[37] will transport energy to the surface layer,[38,39] eventually resulting in thermal equilibration. Hence, we adopt a two-temperature model, one temperature for a substrate and one for the surface layer,

$$\begin{aligned} \mathrm{d}T_{\mathrm{sub}} &= \alpha\, f_{\mathrm{Laser}}(t)\, \mathrm{d}t, \\ \mathrm{d}T_{\mathrm{surf}} &= \frac{1}{\tau}(T_{\mathrm{sub}} - T_{\mathrm{surf}})\mathrm{d}t, \end{aligned} \tag{2}$$

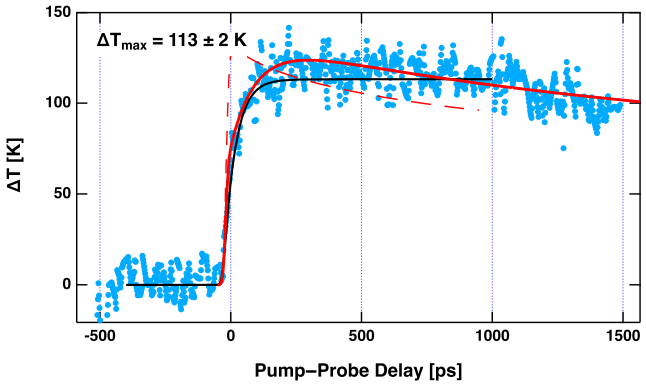

FIG. 1. Temperature transient of the Au film as extracted from the reflectivity changes (experimental data from Ref. 26). The data are fitted by integrating coupled PDEs [Eq. (2)] (black solid line). A more sophisticated light absorption–heat transport model gives the transient (red dashed lines). Only when the hindered heat transport across the interfaces is taken into account is a curve in agreement with the experimental data obtained (red solid line).

where $f_{\mathrm{Laser}}(t)$ describes the temporal laser profile, which is assumed to be a Gaussian (FWHM 19 ps); α is the scaling factor; and τ is the time constant for the energy transfer from the substrate to the surface layer. Fitting the data yields values of 45 ± 16 ps for the transfer time constant and 113 ± 2 K for ΔT_{max}. Note that this model fits the data better than the cumulative distribution function we used in an earlier paper and attempts to reflect the underlying physics better.

Nevertheless, the large time constant warrants some discussion. To gain further insight, we devised a model taking into account the detailed layer structure. The laser light (1) passes through the glass carrier, (2) is partly reflected at the glass Ti interface, (3) is absorbed in the Ti layer, (4) is partly reflected at the Ti/Au interface, (5) is further absorbed in the Au film, (6) is partly reflected at the Au air interface, and (7) the remaining fraction escapes into the surroundings. Along the path at each point, the resulting laser intensity and, from that, the adsorbed energy is calculated. In the second step, the differential equations describing the diffusion of thermal energy are integrated. For details, see the supplementary material. The result is a prediction of the temporal evolution of the sample surface temperature.

That model reproduces the experimentally observed sharp initial rise better but predicts the rise to continue for too long a time, whereas the experimental curve slowly approaches its maximum. This discrepancy can be resolved when the existence of a strong hindrance to heat transfer across the interfaces between the three layers—glass, Ti film, and Au film—is taken into account. *Ad hoc*, claiming that the thermal conductivity is by about two orders of magnitude smaller, a curve fitting the data very well is obtained. This assumption is in line with the large thermal boundary resistance expected for the Au–Ti and Ti–glass interfaces. After the initial period in which light adsorption in the Au film dominates the evolution of the temperature, the continuing rise is due to delayed heat transfer from the Ti layer that is transiently substantially hotter than the Au film. After thermal equilibration between the two metal films, the further evolution is due to heat transfer to the glass substrate. The temperature at the surface slowly decreases again.

This last curve, obtained by this detailed model, will be regarded as representing the temperature of the bath of lattice vibrations with which the adsorbed molecules are interacting and will be used to evaluate the time-resolved spectroscopy data. We regard this as a significant improvement over our earlier work.[26]

B. Spectroscopy

A primary objective of this study was to address the question of which time scale the flash-heated monolayer develops gauche defects. In a well-ordered monolayer of alkylthiol molecules with 12–20 C atoms, the molecules self-assemble into a densely packed structure, in which the individual molecules adopt the all-trans conformation to profit most from intermolecular interactions. In such a 2D crystal, the arrangement of the CH_2 groups is essentially centrosymmetric. This proposition holds if the individual molecules possess an even number of CH_2 entities. However, it is also equally justified, if the number of said entities is odd, on the basis of averaging over domains in which the molecules exhibit different azimuthal orientations. Consequently, the CH_2 stretching vibrations are not discernible in a SF spectrum. This situation changes when the

monolayer is sufficiently heated, thereby enabling individual molecules to form gauche defects.[40,41]

Unfortunately, the literature is ambiguous in its attribution of certain resonances to CH_2 modes, particularly with regard to the Fermi resonance of the symmetric stretch of methylene (d^+_{Fr}) and the anti-symmetric stretch (d^-). While the majority of researchers have claimed that the d^+_{Fr} and d^- modes are found around 2905 and 2925 cm^{-1},[42,43] respectively, Wang and co-workers[44,45] proposed an alternative assignment based on polarization analysis of SF spectra. Some researchers also suggested that the molecule may not exhibit a d^+_{Fr} mode and assigned the signal to a stretch of a terminal CH_2 unit, specifically the one adjacent to the functional headgroup of the molecule.[24,46] In a recent publication, it was suggested that both of these latter resonances belong to different d^- modes, namely, two modes with phases that differ by π, one of which is found around 2881 cm^{-1} and the other around 2913 cm^{-1}.[47] The first mode was only observed by Raman spectroscopy, while the second is only present in IR spectra.

In an attempt to unambiguously resolve this situation, we will discuss the spectra of two related molecules before the ODT spectrum itself is addressed. A clear picture of the spectroscopy and an understanding of the sensitivity of the spectral fit parameter to decisions made when assigning the modes are essential for the data analysis presented later. We opted to record spectra for 11-azidoundecanthiol (AUT). The substitution of the methyl by an azido end group results in the removal of the CH_3 resonances from the spectrum, since the N_3 stretches are located around 2100 cm^{-1} and are not expected to interfere with the CH_2 vibrations. Thus, only the CH_2 modes are observed in the 3000 cm^{-1} spectral region.

Figure 2 shows the vSF spectrum of AUT using the *ppp* polarization combination. Attempts to also utilize the *ssp* combination were fruitless, as the signal was insufficient. In a preliminary analysis of the spectrum, only three resonances, located at 2862, 2905, and 2934 cm^{-1}, were considered. If the phase of the third resonance around 2930 cm^{-1} is permitted to adopt any value, the fit converges in such a way that all three resonances share the identical phase. Thus, one was led to conclude that all three resonances are due to symmetric stretches of the methylene chain CH bonds. If the first and the third resonances are constrained to share an identical phase difference with respect to the non-resonant background, while the phase of the second resonance is permitted to adopt any value, the fit will converge in such a manner that the second resonance's phase differs by 1.3 rad from that of the other two, thus suggesting an anti-symmetric character. This assignment is furthermore consistent with the relative intensities, as the one of the anti-symmetric methylene modes is expected to be lower by at least a factor of 2. Therefore, the resonance around 2905 cm^{-1} is assigned to a d^- mode, and the one around 2934 cm^{-1} to a symmetric mode, more accurately to d^+_{Fr}.

However, it is evident that this initial fit does not represent the data well around 2885 cm^{-1}. Hence, the contribution of an additional mode may be surmised. Indeed, the data in that range are much better represented when an additional mode is incorporated. However, it is observed that the phase difference to the other modes is around π. This finding is at odds with the calculated phases, which suggest a value around 1 rad. This suggests that the additional mode is of anti-symmetric character. Further on, we will designate the new mode as d^-_1 and the one at 2905 cm^{-1} as d^-_2.

The present assignment is at odds with the majority of extant literature that exchanges d^-_2 and d^+_{Fr}.[42] In this context, we would like to direct the reader's attention toward several IR and Raman studies of malonic [$COOH(CH_2)COOH$] and succinic acid [$COOH(CH_2)_2COOH$], which are symmetric molecules with one or two methylene units separating the carbonyl groups. The aforementioned studies report the presence of two methylene resonances: one assigned to the d^+ and the other to the d^- mode. The separation between these is ≈40–50 cm^{-1}, which is comparable to the separation between the present assignment's d^+ and d^-_2 modes.

In order to gain further insights facilitating the band assignment, IR and Raman spectra of powder samples were recorded. Figure 3 shows the IR and Raman spectra of AUT along with the Raman spectrum of 11-mercapto-1-undecanol (MUO), which we recorded as the AUT exhibited strong water signals as the powder drew moisture. The first resonance is found in the IR and Raman spectra at 2850 cm^{-1}, and in accordance with the literature, it is assigned to the d^+ mode. This suggests a red shift of 13 cm^{-1} with respect to the SF spectrum of an alkylthiol monolayer. For the moment, the strong Raman signal at 2884 cm^{-1} will

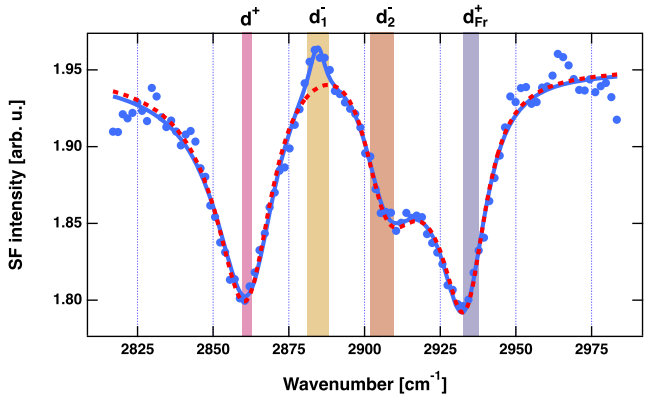

FIG. 2. vSF spectrum of AUT (11-azidoundecanethiol) deposited on 30 nm Au/13 nm Ti obtained using the *ppp* polarization combination. The blue line represents a fit to the data with four resonances (d^+, d^-_1, d^-_2, and d^+_{Fr}), and the dotted red line represents a fit with three resonances, i.e., lacking the d^-_1 one.

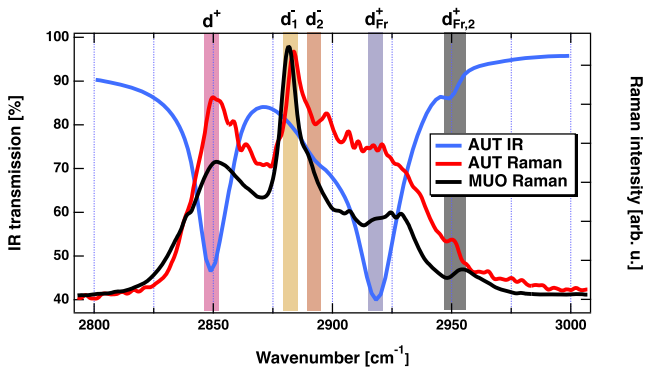

FIG. 3. IR and Raman spectra of AUT (11-azido-undecanthiol) and MUO (11-mercapto-undecanol). The spectra were acquired from powder samples.

not be considered. The IR spectrum displays a weak feature at 2893 cm^{-1}, which is again offset by 13 cm^{-1} relative to the d_2^- feature in the SF spectrum. The IR spectrum exhibits a strong band at 2918 cm^{-1}, i.e., 16 cm^{-1} to the red of the feature in the SF spectrum that we assigned to the d_{Fr}^+ mode, and finally, a resonance is observed at 2950 cm^{-1}. As proposed by Lu *et al.*,[45] this absorption could be attributed to another d_{Fr}^+ mode. Inspecting the SF spectrum around 2965 cm^{-1}, where it would be expected, we identify a possible signal. However, that signal is too small to allow for a firm confirmation.

To summarize, we find all modes observed by SFS also again in the IR or Raman spectrum; however, they are red shifted by 13–16 cm^{-1}. The aforementioned signal at 2884 cm^{-1} is the sole exception to this rule. However, its position almost perfectly coincides with the feature we have designated as d_1^-.

The insights gained from dissecting the AUT spectra allow us a robust interpretation of the vSF spectrum of ODT (Fig. 4). We settled on fitting the spectra assuming six relevant resonances (Table I). (Details are laid out in the supplementary material.) However, it is noteworthy that the intensities of the r^+ and r^- modes—which we will use in the further data analysis—are rather independent from the number of further resonances accounted for in the fit. The additional features that significantly improve the fit were found at 2855, 2905, and 2925 cm^{-1}. The mode at 2905 cm^{-1} also appears in the AUT spectrum with the identical phase difference of 1, suggesting it should be identified as a second d^- mode.

A comparison of the *ssp* and *ppp* spectra of ODT (Fig. 4) reveals that the d^+, r^+, and r_{Fr}^+ modes are found at identical wavenumbers. However, the position of the r^- mode differs by 7 cm^{-1}, which was already reported by Bordenyuk *et al.*[48] It may be speculated that this is the splitting between the in-plane and out-of-plane components of the anti-symmetric stretch moiety. Note that the equations describing the amplitude are identical for both r^- modes.

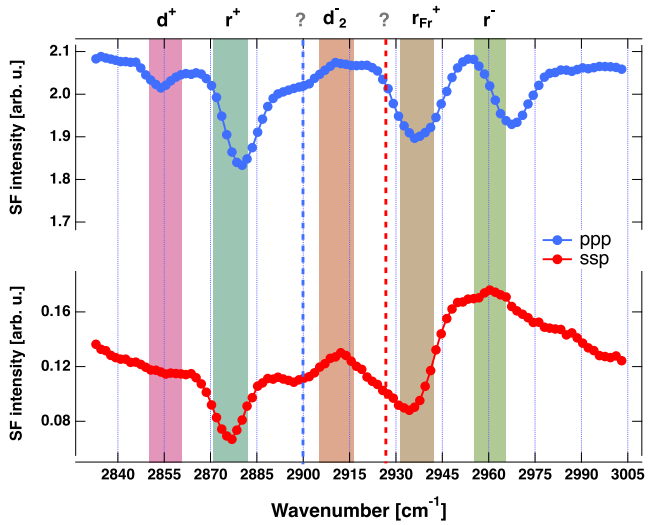

FIG. 4. vSF spectra of ODT on 30 nm Au/13 nm Ti obtained using the *ppp* and *ssp* polarization combinations. The solid lines connecting the data points serve as guides to the eye.

TABLE I. Summary of the fitting parameters extracted. d^+, r^+, and r_{Fr}^+ and the unassignable modes share the same phase difference to the nonresonant background, while the phase differences of d_2^- and r^- are offset by π.

Parameter	*ppp*	*ssp*
ω_{d^+} (cm^{-1})	2853 ± 1	2854 ± 3
ω_{r^+} (cm^{-1})	2880 ± 0	2876 ± 1
$\omega_?$ (cm^{-1})		2899 ± 3
$\omega_{d_2^-}$ (cm^{-1})	2904 ± 2	2912 ± 2
$\omega_?$ (cm^{-1})	2925 ± 2	
$\omega_{r_{Fr}^+}$ (cm^{-1})	2937 ± 1	2935 ± 1
ω_{r^-} (cm^{-1})	2963 ± 1	2955 ± 4
Γ_{d^+} (cm^{-1})	4.6 ± 1.7	4 (set)
Γ_{r^+} (cm^{-1})	6.3 ± 0.7	6.5 ± 0.9
$\Gamma_?$ (cm^{-1})		6.5 ± 5.8
$\Gamma_{d_2^-}$ (cm^{-1})	11.9 ± 4.2	3.2 ± 3.4
$\Gamma_?$ (cm^{-1})	3 ± 4.2	
$\Gamma_{r_{Fr}^+}$ (cm^{-1})	11.0 ± 0.9	10.6 ± 2
Γ_{r^-} (cm^{-1})	6.6 ± 0.9	19.7 ± 2.9
$\chi_{NR}^{(2)}$ (arb. u.)	1.45 ± 0.00	0.36 ± 0.01
ϕ (rad)	1.56 ± 0.07	1.59 ± 0.24

C. Flash heating

Figures 5 and 6 display the series of vSF spectra obtained when flash heating the samples for varied delays between pump and probe laser pulses. In the flash-heated experiment, the development of the spectra with delay is qualitatively rather similar to that observed when statically heating the sample. We regard the differing absolute intensity as an experimental artifact, likely due to slightly different experimental conditions. Detailed inspection reveals the dynamics we are interested in.

Figure 5 shows the remaining molecular intensity observed for various modes as a function of the pump–probe delay. Data are available from spectra using the *ppp* and *ssp* polarization combinations. It is obvious that the response of the vSF signal is delayed when compared to the evolution of the substrate temperature (see the top left panel).

D. Dynamics

We assume that the intensity of the molecular signal decreases linearly with temperature over the range studied. Hence, we can take the molecular intensity directly as a proxy for the temperature of the molecule—or more precisely, for the temperature relevant for the particular mode we are studying. In Sec. III A, we derived a curve describing the evolution of substrate surface temperature. Hence, we can formulate a two-temperature model coupling the sample temperature, T_{sub}, with the molecular vSF intensity, I_{mol},

$$dI_{mol} = (B\,T_{sub} - I_{mol})\,\frac{1}{\tau}\,dt, \tag{3}$$

where B serves to scale the temperature effects on the two quantities. τ is the time constant for the equilibration in temperatures between

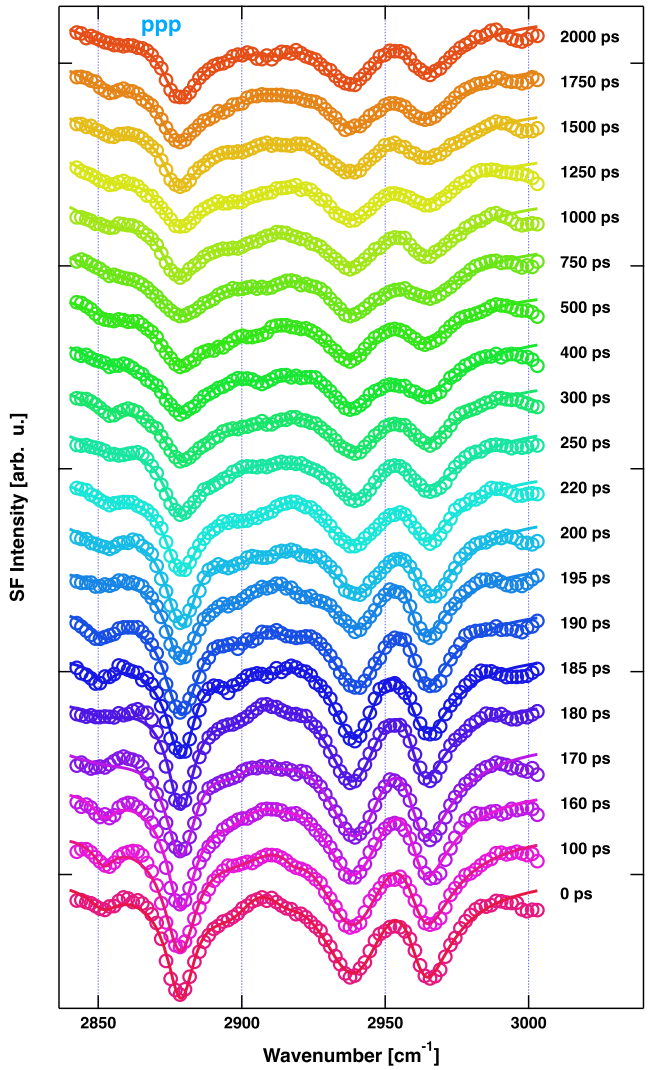

FIG. 5. vSF spectra of ODT recorded using the *ppp* polarization combination at different delay line positions between the pump and the probe. The solid lines represent the fits to the data. The indicated delays were calibrated by fitting the data shown in Fig. 7.

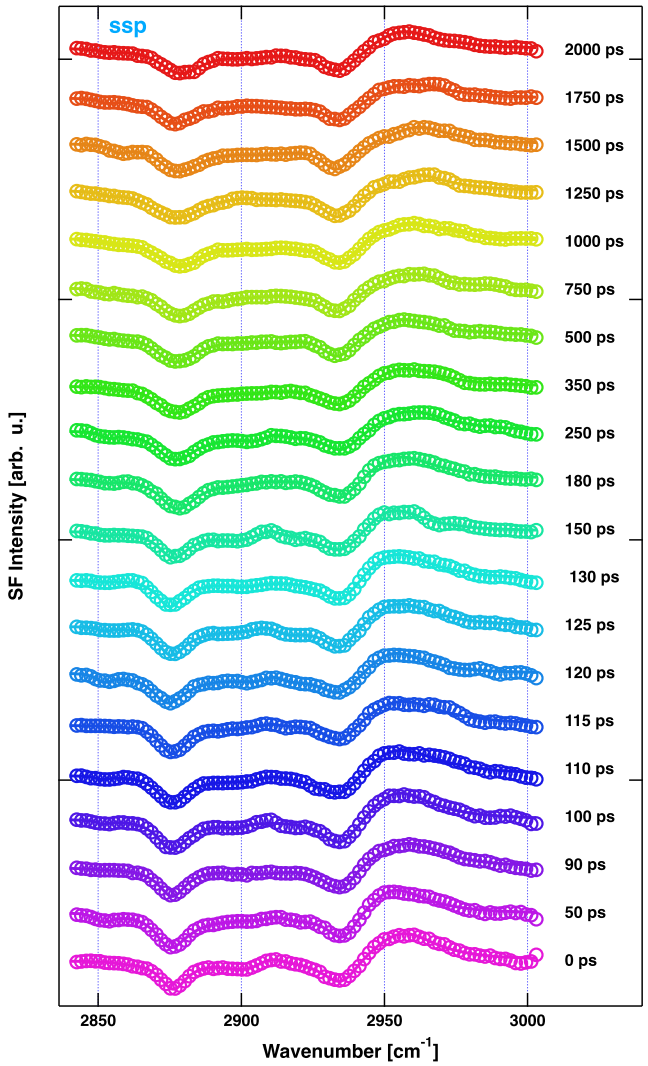

FIG. 6. vSF spectra of ODT, recorded using the *ssp* polarization combination at different delays between the pump and probe. The solid lines represent the fits to the data. The indicated delays were calibrated by fitting the data shown in Fig. 7.

the substrate and the molecular intensity of the particular mode of ODT.

The parameters B, τ, and $I_{mol}(t = 0\ \mathrm{s})$ were fit using a least-squares optimization algorithm. Moreover, the delay line position corresponding to a delay of 0 ps was a further free parameter. Thus, we used the fit to also calibrate the offset of the delay scale. In the graph, a delay of 0 ps corresponds now to the situation where the peak intensities of all laser beams coincide in time on the sample. Despite our choice to allow the offset of the delay axis to float freely, all fits settled within ±2 ps on the same value for the zero point. Only for the *ppp* data on the r^+ mode does the zero offset in time seem less well defined, which corresponds with the result that also the time constant τ carries a large uncertainty in this case.

The data for r^+, r^-, and r^+_{Fr} are well presented by the fit curves. Admittedly, the *ppp* data for the r^+_{Fr} mode allow for an excessively large range of interpretation, such that we regard this experiment as inconclusive. The other datasets yield values for the coupling time constant between 94 and 153 ps. Taking into account the obtained uncertainties, we see that the value ranges overlap. Hence, we conclude that for these three modes, τ is uniformly about 125 ps. It is worth noting that the relative signal attenuation, B/I_0, is different for the r^+ and r^- modes but with similar error margins when studied using the *ppp* or *ssp* polarization combination.

The situation is different for the data on the d modes. The data are characterized by an increase in intensity—that is, no problem for the fit—with a time constant of ~25 ps, i.e., much faster than observed for the other modes. However, the intensity increase

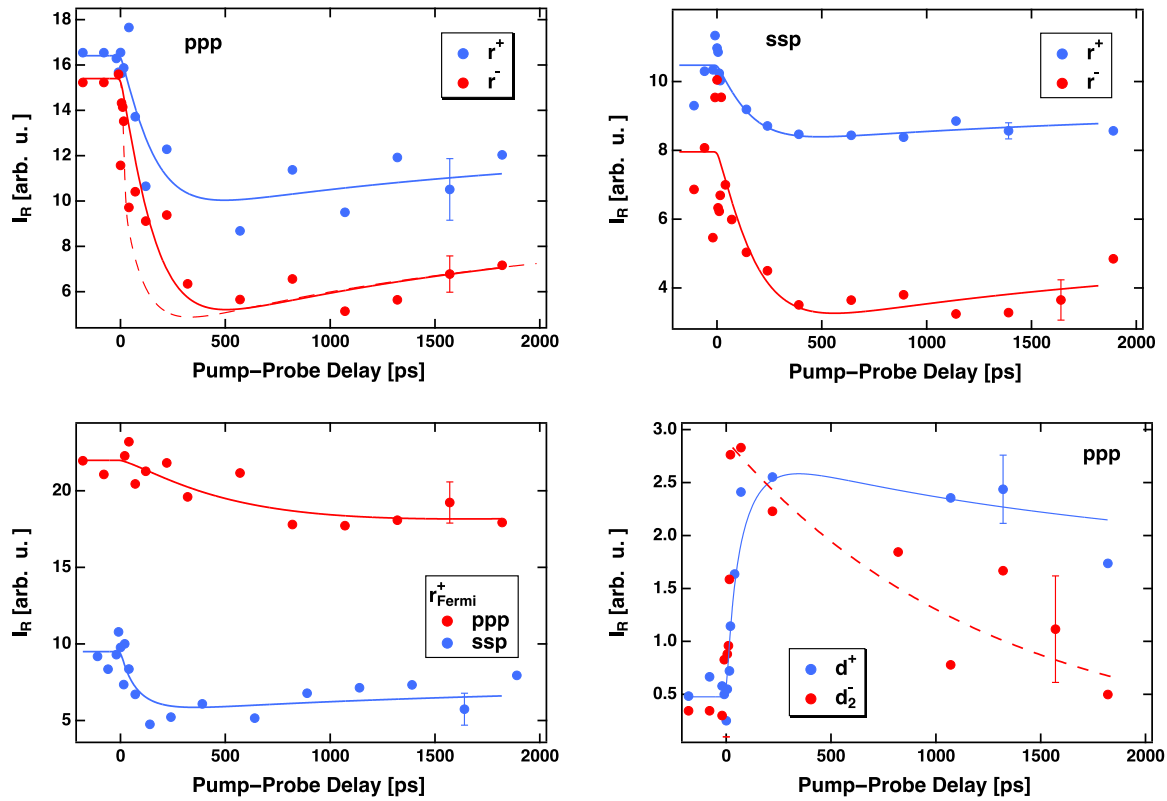

FIG. 7. Evolution of the molecular SF intensity as a function of the pump–probe delay. Top left: remaining intensity for the r^+ and r^- modes recorded in *ppp*. The dashed line indicates the intensity expected, provided it follows without lag the substrate temperature. Top right: remaining intensity for the r^+ and r^- modes recorded in *ssp*. Bottom left: remaining intensity for the r^+_{Fr} mode recorded in *ppp* and *ssp*. Bottom right: remaining intensity for the d^+ and d_2^- modes recorded in *ppp*. The dashed line indicates an exponential decay fitted to the d_2^- data with a time constant of 1250 ps. The solid lines represent fits using the model formulated in Eq. (3). The error bars represent the estimates of the uncertainties in the relative intensities, ignoring systematic errors. The position of the zero delay was derived from the fit result. The fit results are listed in Table II.

observed for the d_2^- mode disappears faster than the temperature of the substrate returns to its idle value. A simple exponential fit to this trailing transient yields a time constant of about 1250 ps. The model we devised fails to explain this evolution of the molecular intensity as a function of pump–probe delay.

E. Geometry change

It is well established that spectra of the kind we have here can be used to gain insight into the adsorption geometry of the molecules in the ordered layer at the surface. For this purpose, we evaluate the ratio of the molecular intensities observed for the r^+ and r^- modes. The dependence of these on the tilt angle of the symmetry axis of the CH_3 group with respect to the surface normal can be calculated following earlier work.[44,49–51] We carried out this evaluation for both datasets, as we have *ppp* and *ssp* spectra available, which will serve as an internal consistency check. Studies frequently simplify the analysis by assuming a δ-distribution in tilt angles. However, this appears to us as an oversimplification. At least under the flash-heated conditions, thermal energy will allow the molecules to perform pendulum motions if gauche defects are not also formed. Nevertheless, we assume azimuthal isotropy in view of the mm spot size we sample. Hence, we assume a Gaussian distribution of tilt angles centered around the mean of one with a width, σ. Calculation of the expected intensity as a function of the tilt angle for various assumed values of σ and both polarization components can be found in the supplementary material.

In a previous publication, we evaluated the ratio of the molecular intensities of a single mode observed when using the *ppp* or *ssp* polarization combination to gain insight into the adsorption geometry of the molecule and its change after flash-heating. In this study, we had to adopt a different approach. We followed Hirose[49,52] and Wang *et al.*[50] to calculate the intensities. The result is that the intensities of the r^+ mode for *ssp* and *ppp* should differ by a factor of 0.1. In contrast, the experimental values suggest an intensity ratio of 1, considering error margins, or 0.5 at the lowest. At present, we have no explanation for this stark discrepancy. However, we note that several other experimentalists report data consistent with our own.[53–55] Of course, the calculated numbers are dependent on the value used for the refractive indices of Au and the adlayer as well as the Raman depolarization ratio, ρ, which are associated with considerable uncertainties. However, exploring a range of conceivable

TABLE II. Compilation of fit results and errors (confidence interval = 1σ) of the profiles in Fig. 7 to Eq. (3).

		τ (ps)	B/I_0 ($\times 10^3$)	t_0 (ps)
ppp	r^+	94 ± 78	9.5 ± 1.0	150 ± 72
	r^-	119 ± 15	19.3 ± 2.4	150 ± 0.1
	r^+_{Fr}	608 ± 150	5.2 ± 1.3	150 ± 0.7
	d^+	24 ± 4	−126 ± 65	150 ± 0.1
ssp	r^+	153 ± 30	7.9 ± 0.5	150 ± 0.1
	r^-	123 ± 37	14.8 ± 1.5	150 ± 0.2
	r^+_{Fr}	40 ± 12	11.4 ± 2.7	150 ± 0.1

values, we do not find a solution to this puzzle. Hence, we refrain from basing our data evaluation on the ratios of the different intensities of modes observed in the *ssp* and *ppp* spectra. Instead, we use the intensity ratios between the r^+ and r^- modes in either the *ssp* or, alternatively, the *ppp* spectrum.

Following a procedure that we presented in detail in an earlier paper,[26] we combine various intensity ratios to find constraints on the possible adsorption geometry. However, there are at least two unknown quantities to consider: (*i*) the mean tilt angle and (*ii*) the width of the distribution around the mean value. Therefore, we assign values to the width, σ, and determine the range of tilt angles consistent with the experimental data, accounting for the error margins of the experimental intensities. Combining several of these arguments, we derive the graph shown in Fig. 8. For further details, the reader is referred to the supplementary material.

Figure 8 indicates that, under idle conditions, the mean tilt angle of the methyl head group is around 66° ± 7°, provided the spread, σ, around the mean value due to thermal fluctuations is not large (≤7°). This is entirely consistent with the data reported from GIXD measurements, suggesting a mean tilt angle of the symmetry axis of the alkyl chain of ~30°. Note that the geometry analysis of the SFS data does not yield this angle but rather the tilt angle of the symmetry axis of the molecular group to which the mode belongs, on which the analysis is based—in our case, the CH_3 group. This group is inclined by 36° with respect to the axis of an alkane molecule (Fig. 9). Rotation around this axis is hindered by the bond of the thiol group to the surface. Hence, for alkyl thiol molecules with an even number of C-atoms in an ordered monolayer, the tilt angle of the methyl group with respect to the surface normal is 36° larger than the tilt angle of the alkyl skeleton. Therefore, we find perfect agreement. Note that the small variation of the mean tilt angle for assumed widths smaller than 7° also suggests that, in this case, it is not a mistake to work with a δ-distribution in widths for the formal analysis, as it is a frequent practice).

Following flash heating, the situation is different. The graph shows that, if we assume a small σ_f, an increase in the mean tilt angle is suggested when compared to idle conditions. We cannot see a physical scenario consistent with such an evolution, given that the tilt angle is constrained by the mutual repulsion of the molecules in the monolayer. Furthermore, thermal energy should lead to greater disorder. In view of the overlap of the error ranges for θ_i and θ_f, one might wonder at first glance whether there must be a change at all. However, (*i*) the vSF spectrum changes markedly, and (*ii*) the θ value in the overlap region is inconsistent with the GIXD data. Therefore, we consider an increase in σ from initially 0°–8° to finally 16°–23° to be more likely. In this hypothesis, the mean tilt may increase somewhat, with the spread reflecting large-angle pendulum motions. This interpretation is qualitatively in agreement and quantitatively close to what has been suggested from molecular dynamics simulations.[21]

The fast and rather short-lived increase in intensity observed for the d^- modes is one puzzling finding. It is tempting to interpret this as an indication of gauche defects forming, as this is an

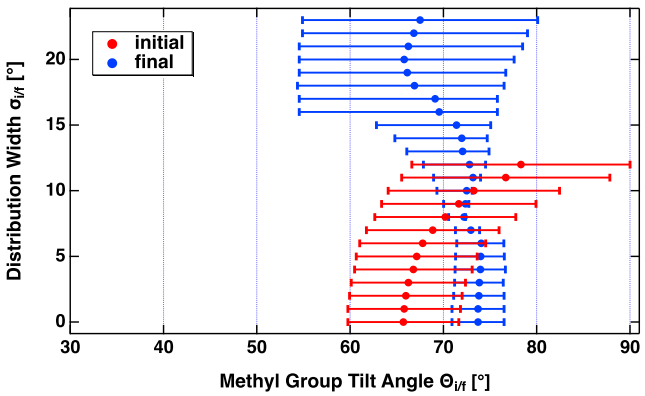

FIG. 8. Ranges of the possible mean tilt angle of the CH_3 group with respect to the surface normal before, θ_i, and after, θ_f, flash heating the sample. Values have been determined for all values for the width of the distribution consistent with the intensities of the r^+ and r^- mode spectra. Note: The horizontal error bars indicate the uncertainty margins of the mean tilt angle when assuming a given width of the distribution, σ. θ_i and θ_f refer to the tilt angle under room temperature, i.e., idle, conditions and after flash heating, respectively. σ_i and σ_f refer to the corresponding widths.

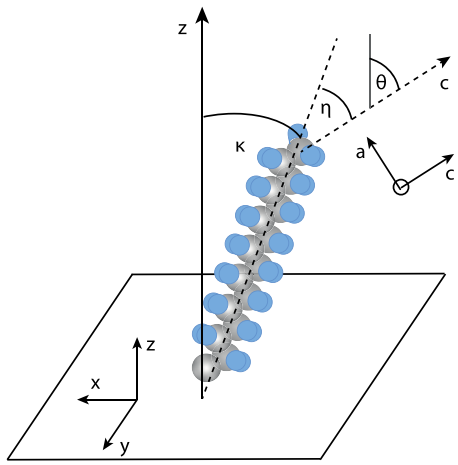

FIG. 9. Illustration of the geometry of ODT in the ordered layer in all-trans conformation. The molecular symmetry axis is inclined by κ with respect to the surface normal, *z*. The methyl group is inclined by η with respect to the molecule's symmetry axis. θ is the angle of the symmetry axis of the methyl group with respect to the surface normal. As rotation around the S–CH_2 bond is hindered, θ is unambiguously defined. For alkylthiols with an even number of CH_2-groups, θ is by 36° larger than κ.

established concept in the interpretation of spectra recorded under steady-state conditions. However, it is difficult to accept that gauche defects are building up faster than the temperature in the layer is rising. It may, however, be speculated that the loss of the molecules' overall inclined geometry reduces the coherence of the polarization responsible for the intensity of the d^- modes. Hence, we refrain from suggesting an answer to the question of the timescale of gauche defect formation, as the data are inconclusive.

IV. SUMMARY

The response of a monolayer of octadecylthiol adsorbed on a thin Au film to flash heating was studied. A 19 ps laser pulse with a wavelength of 532 nm was used to rapidly heat a 13 nm Ti/30 nm Au heterostructure by passing it from the backside through the glass support. The surface temperature is monitored by recording the optical reflectivity. Modeling of the temperature transient taking into account the detailed structure and heat transfer properties of the metal layers reproduces the observed transient well. Within 100 ps, a peak temperature rise of ~100 K is achieved. Vibrational sum frequency spectroscopy was employed to characterize the evolution of the molecular adsorption geometry. For the idle temperature, 300 K, the results agree well with earlier conclusions from GIXD, namely, an inclination of the molecules in an ordered structure by ~30°. For the flash-heated layer, a large loss of order is evident in the SF spectrum, indicating a large spread of individual tilt angles. The evolution of the molecular order lags by around 125 ps with respect to the temperature rise induced in the metal substrate.

SUPPLEMENTARY MATERIAL

See the supplementary material for details on the analysis of the vSF spectra.

ACKNOWLEDGMENTS

E.H. acknowledges the funding from the Deutsche Forschungsgemeinschaft (DFG, German Research Foundation), Project No. 278162697, within CRC 1242 "Non-Equilibrium Dynamics of Condensed Matter in the Time Domain." We thank Nelli Kremer and Tim Lämmerzahl for their valuable discussions and acknowledge contributions during the initial stages of the experiment by Damian Firla, Andre Beier-Hannweg, and Joshua Multhaup.

AUTHOR DECLARATIONS

Conflict of Interest

The authors have no conflicts to disclose.

Author Contributions

Matthias Linke: Conceptualization (supporting); Data curation (equal); Formal analysis (lead); Investigation (lead); Visualization (equal); Writing – review & editing (equal). **Eckart Hasselbrink**: Conceptualization (lead); Data curation (equal); Formal analysis (supporting); Funding acquisition (lead); Project administration (lead); Resources (equal); Supervision (lead); Visualization (equal); Writing – original draft (lead); Writing – review & editing (equal).

DATA AVAILABILITY

The data that support the findings of this study are available from the corresponding author upon reasonable request.

REFERENCES

[1] A. Ulman, "Formation and structure of self-assembled monolayers," Chem. Rev. **96**, 1533 (1996).
[2] F. Schreiber, "Structure and growth of self-assembling monolayers," Prog. Surf. Sci. **65**, 151 (2000).
[3] J. C. Love, L. A. Estroff, J. K. Kriebel, R. G. Nuzzo, and G. M. Whitesides, "Self-assembled monolayers of thiolates on metals as a form of nanotechnology," Chem. Rev. **105**, 1103–1170 (2005).
[4] R. G. Nuzzo and D. L. Allara, "Adsorption of bifunctional organic disulfides on gold surfaces," J. Am. Chem. Soc. **105**, 4481 (1983).
[5] C.-L. Liao, S. M. Faizanuddin, J. Haruyama, W.-S. Liao, and Y.-C. Wen, "Effects of chain–chain interaction on the configuration of short-chain alkanethiol self-assembled monolayers on a metal surface," J. Chem. Phys. **160**, 214711 (2024).
[6] L. Strong and G. M. Whitesides, "Structures of self-assembled monolayer films of organosulfur compounds adsorbed on gold single crystals: Electron diffraction studies," Langmuir **4**, 546 (1988).
[7] S. D. Evans, K. E. Goppert-Berarducci, E. Urankar, L. J. Gerenser, A. Ulman, and R. G. Snyder, "Monolayers having large in-plane dipole moments: Characterization of sulfone-containing self-assembled monolayers of alkanethiols on gold by Fourier transform infrared spectroscopy, x-ray photoelectron spectroscopy and wetting," Langmuir **7**, 2700 (1991).
[8] M. D. Porter, T. B. Bright, D. L. Allara, and C. E. D. Chidsey, "Spontaneously organized molecular assemblies. 4. Structural characterization of n-alkyl thiol monolayers on gold by optical ellipsometry, infrared spectroscopy, and electrochemistry," J. Am. Chem. Soc. **109**, 3559 (1987).
[9] C. E. D. Chidsey, G.-Y. Liu, P. Rowntree, and G. Scoles, "Molecular order at the surface of an organic monolayer studied by low energy helium diffraction," J. Chem. Phys. **91**, 4421 (1989).
[10] G. J. Kluth, M. Sander, M. M. Sung, and R. Maboudian, "Study of the desorption mechanism of alkylsiloxane self-assembled monolayers through isotopic labeling and high resolution electron energy-loss spectroscopy experiments," J. Vac. Sci. Technol. A **16**, 932 (1998).
[11] G. E. Poirier and M. J. Tarlov, "The c(4 × 2) superlattice of n-alkanethiol monolayers self-assembled on Au(111)," Langmuir **10**, 2853 (1994).
[12] M. G. Samant, C. A. Brown, and J. G. Gordon, "Formation of an ordered self-assembled monolayer of docosaneselenol on gold(111). Structure by surface x-ray diffraction," Langmuir **8**, 1615–1618 (1992).
[13] M. S. Yeganeh, S. M. Dougal, R. S. Polizzotti, and P. Rabinowitz, "Interfacial atomic structure of a self-assembled alkyl thiol monolayer/Au(111): A sum-frequency generation study," Phys. Rev. Lett. **74**, 1811 (1995).
[14] M. Kawasaki and H. Nagayama, "Observation of highly ordered 3 × 4 phase of ethanethiol self-assembled monolayer on Au(111)," Chem. Lett. **30**, 942 (2001).
[15] P. E. Laibinis, G. M. Whitesides, D. L. Allara, Y. T. Tao, A. N. Parikh, and R. G. Nuzzo, "Comparison of the structures and wetting properties of self-assembled monolayers of n-alkanethiols on the coinage metal surfaces, copper, silver, and gold," J. Am. Chem. Soc. **113**, 7152 (1991).
[16] P. Fenter, A. Eberhardt, K. S. Liang, and P. Eisenberger, "Epitaxy and chain-length dependent strain in self-assembled monolayers," J. Chem. Phys. **106**, 1600 (1997).
[17] O. Dannenberger, K. Weiss, H.-J. Himmel, B. Jäger, M. Buck, and C. Wöll, "An orientation analysis of differently endgroup-functionalised alkanethiols adsorbed on Au substrates," Thin Solid Films **307**, 183 (1997).
[18] M. G. Roper, M. P. Skegg, C. J. Fisher, J. J. Lee, V. R. Dhanak, D. P. Woodruff, and R. G. Jones, "Atop adsorption site of sulphur head groups in gold-thiolate self-assembled monolayers," Chem. Phys. Lett. **389**, 87–91 (2004).
[19] P. Maksymovych, O. Voznyy, D. B. Dougherty, D. C. Sorescu, and J. T. Yates, "Gold adatom as a key structural component in self-assembled monolayers of organosulfur molecules on Au(111)," Prog. Surf. Sci. **85**, 206–240 (2010).

[20]X. Torrelles, E. Pensa, E. Cortés, R. Salvarezza, P. Carro, C. Hernández Guerrero, C. Ocal, E. Barrena, and S. Ferrer, "Solving the long-standing controversy of long-chain alkanethiols surface structure on Au(111)," J. Phys. Chem. C **122**, 3893–3902 (2018).
[21]W. Mar and M. L. Klein, "Molecular dynamics study of the self-assembled monolayer composed of $S(CH_2)_{14}CH_3$ molecules using an all-atoms model," Langmuir **10**, 188 (1994).
[22]F. Schreiber, M. C. Gerstenberg, H. Dosch, and G. Scoles, "Melting point enhancement of a self-assembled monolayer induced by a van der Waals bound capping layer," Langmuir **19**, 10004 (2003).
[23]M. Buck and M. Himmelhaus, "Vibrational spectroscopy of interfaces by infrared–visible sum frequency generation," J. Vac. Sci. Technol. A **19**, 2717–2736 (2001).
[24]M. Himmelhaus, F. Eisert, M. Buck, and M. Grunze, "Self-assembly of *n*-alkanethiol monolayers. A study by IR-visible sum frequency spectroscopy (SFG)," J. Phys. Chem. B **104**, 576–584 (2000).
[25]F. Cecchet, D. Lis, J. Guthmuller, B. Champagne, Y. Caudano, C. Silien, A. Addin Mani, P. A. Thiry, and A. Peremans, "Orientational analysis of dodecanethiol and *p*-nitrothiophenol SAMs on metals with polarisation dependent SFG spectroscopy," ChemPhysChem **11**, 607 (2010).
[26]M. Linke, J. Multhaup, and E. Hasselbrink, "Response of a 4-nitrothiophenol monolayer to rapid heating studied by vibrational sum frequency spectroscopy," J. Chem. Phys. **161**, 194711 (2024).
[27]Z. Wang, J. A. Carter, A. Lagutchev, Y. K. Koh, N.-H. Seong, D. G. Cahill, and D. D. Dlott, "Ultrafast flash thermal conductance of molecular chains," Science **317**, 787 (2007).
[28]Z. Wang, D. G. Cahill, J. A. Carter, Y. K. Koh, A. Lagutchev, N.-H. Seong, and D. D. Dlott, "Ultrafast dynamics of heat flow across molecules," Chem. Phys. **350**, 31 (2008).
[29]J. Hekele, M. Linke, T. Keller, J. Jose, M. Hille, E. Hasselbrink, S. Schlücker, and P. Kratzer, "A fresh look at the structure of aromatic thiols on Au surfaces from theory and experiment," J. Chem. Phys. **155**, 044707 (2021).
[30]A. Beran, "The reflectance behaviour of gold at temperatures up to 500 °C," TMPM, Tschermaks Mineral. Petrogr. Mitt. **34**, 211 (1985).
[31]F. Vidal and A. Tadjeddine, "Sum-frequency generation spectroscopy of interfaces," Rep. Prog. Phys. **68**, 1095–1127 (2005).
[32]B. Busson and A. Tadjeddine, "Non-uniqueness of parameters extracted from resonant second-order nonlinear optical spectroscopies," J. Phys. Chem. C **113**, 21895 (2009).
[33]S. I. Anisimov, B. L. Kapeliovich, and T. L. Perel'man, "Emission of electrons from the surface of metals induced by ultrashort laser pulses," Zh. Eksp. Theo. Fiz. **66**, 776 (1974), http://www.jetp.ras.ru/cgi-bin/dn/e_039_02_0375.pdf.
[34]J. M. Hicks, L. E. Urbach, E. W. Plummer, and H.-L. Dai, "Can pulsed laser excitation of surfaces be described by a thermal model?," Phys. Rev. Lett. **61**, 2588 (1988).
[35]M. Bauer, A. Marienfeld, and M. Aeschlimann, "Hot electron lifetimes in metals probed by time-resolved two-photon photoemission," Prog. Surf. Sci. **90**, 319 (2015).
[36]M. Volkov, S. A. Sato, F. Schlaepfer, L. Kasmi, N. Hartmann, M. Lucchini, L. Gallmann, A. Rubio, and U. Keller, "Attosecond screening dynamics mediated by electron localization in transition metals," Nat. Phys. **15**, 1145–1149 (2019).
[37]M. Heckschen, Y. Beyazit, E. Shomali, F. Kühne, J. Jayabalan, P. Zhou, D. Diesing, M. E. Gruner, R. Pentcheva, A. Lorke, B. Sothmann, and U. Bovensiepen, "Spatio-temporal electron propagation dynamics in Au/Fe/MgO(001) in nonequilibrium: Revealing single scattering events and the ballistic limit," PRX Energy **2**, 043009 (2023).
[38]T. Q. Qiu and C. L. Tien, "Femtosecond laser heating of multi-layer metals—I. Analysis," Int. J. Heat Mass Transfer **37**, 2789–2797 (1994).
[39]D. Y. Tzou and K. S. Chiu, "Temperature-dependent thermal lagging in ultrafast laser heating," Int. J. Heat Mass Transfer **44**, 1725–1734 (2001).
[40]J. Weber, T. Balgar, and E. Hasselbrink, "Conformational disorder in alkylsiloxane monolayers at elevated temperatures," J. Chem. Phys. **139**, 244902 (2013).
[41]J. Weber, A. Beier, E. Hasselbrink, and T. Balgar, "Thermally induced conformational changes of Ca-arachidate Langmuir-Blodgett films at different compression," J. Chem. Phys. **141**, 044912 (2014).
[42]J. C. Conboy, M. C. Messmer, and G. L. Richmond, "Dependence of alkyl chain conformation of simple ionic surfactants on head group functionality as studied by vibrational sum-frequency spectroscopy," J. Phys. Chem. B **101**, 6724–6733 (1997).
[43]S. Hosseinpour, J. Hedberg, S. Baldelli, C. Leygraf, and M. Johnson, "Initial oxidation of alkanethiol-covered copper studied by vibrational sum frequency spectroscopy," J. Phys. Chem. C **115**, 23871–23879 (2011).
[44]H.-F. Wang, "Sum frequency generation vibrational spectroscopy (SFG-VS) for complex molecular surfaces and interfaces: Spectral lineshape measurement and analysis plus some controversial issues," Prog. Surf. Sci. **91**, 155–182 (2016).
[45]R. Lu, W. Gan, B.-H. Wu, H. Chen, and H.-F. Wang, "Vibrational polarization spectroscopy of CH stretching modes of the methylene group at the vapor/liquid interfaces with sum frequency generation," J. Phys. Chem. B **108**, 7297 (2004).
[46]M. Lackner, "Tracking vibrational dynamics: Time-resolved 2-color vibrational sum-frequency spectroscopy of calcium arachidate adsorbate layers," Ph.D. thesis, Universität Duisburg-Essen, 2021.
[47]M. Marquardt, "Unravelling the energy flow: Probing vibrational dynamics in non-equilibrium alkyl chain monolayers using sum-frequency spectroscopy," Ph.D. thesis, Universität Duisburg-Essen, 2023.
[48]A. N. Bordenyuk, C. Weeraman, and A. V. Benderskii, "Sum frequency generation from alkanethiol capped metallic nanoparticles and vibrational mode specific enhancement in nanoparticle aggregates," Proc. SPIE **6641**, 66410C (2007).
[49]C. Hirose, N. Akamatsu, and K. Domen, "Formulas for the analysis of the surface SFG spectrum and transformation coefficients of Cartesian SFG tensor components," Appl. Spectrosc. **46**, 1051–1072 (1992).
[50]H.-F. Wang, W. Gan, R. Lu, Y. Rao, and B.-H. Wu, "Quantitative spectral and orientational analysis in surface sum frequency generation vibrational spectroscopy (SFG-VS)," Int. Rev. Phys. Chem. **24**, 191 (2005).
[51]H.-F. Wang, L. Velarde, W. Gan, and L. Fu, "Quantitative sum-frequency generation vibrational spectroscopy of molecular surfaces and interfaces: Lineshape, polarization, and orientation," Annu. Rev. Phys. Chem. **66**, 189 (2015).
[52]C. Hirose, N. Akamatsu, and K. Domen, "Formulas for the analysis of surface sum-frequency generation spectrum by CH stretching modes of methyl and methylene groups," J. Chem. Phys. **96**, 997–1004 (1992).
[53]C. M. Berg, A. Lagutchev, and D. D. Dlott, "Probing of molecular adsorbates on Au surfaces with large-amplitude temperature jumps," J. Appl. Phys. **113**, 183509 (2013).
[54]N. M. Adhikari, U. I. Premadasa, Z. J. Rudy, and K. L. A. Cimatu, "Orientational analysis of monolayers at low surface concentrations due to an increased signal-to-noise ratio (S/N) using broadband sum frequency generation vibrational spectroscopy," Appl. Spectrosc. **73**, 1146–1159 (2019).
[55]D. Firla, "Summenfrequenzspektroskopische Untersuchungen des Temperatureinflusses auf die Struktur von organischen Monoschichten mit unterschiedlichen Ankergruppen," Ph.D. thesis, Universität Duisburg-Essen, 2022.